Active Microwave Imaging I—2-D Forward and Inverse Scattering Methods

Qing Huo Liu, *Senior Member, IEEE*, Zhong Qing Zhang, *Senior Member, IEEE*, Tonghui T. Wang, J. A. Bryan, Gary A. Ybarra, *Member, IEEE*, Loren W. Nolte, *Life Senior Member, IEEE*, and William T. Joines, *Life Senior Member, IEEE*

***Abstract*—Active microwave imaging (MWI) for the detection of breast tumors is an emerging technique to complement existing X-ray mammography. The potential advantages of MWI arise mainly from the high contrast of electrical properties between tumors and normal breast tissue. However, this high contrast also increases the difficulty of forming an accurate image because of increased multiple scattering. To address this issue, we develop fast forward methods based on the combination of the extended Born approximation, conjugate- and biconjugate-gradient methods, and the fast Fourier transform. We propose two nonlinear MWI algorithms to improve the resolution for the high-contrast media encountered in microwave breast-tumor detection. Numerical results show that our algorithms can accurately model and invert for the high-contrast media in breast tissue. The outcome of the inversion algorithms is a high-resolution digital image containing the physical properties of the tissue and potential tumors.**

***Index Terms*—Biomedical applications, fast algorithms, imaging, inverse scattering, microwave techniques.**

I. Introduction

EARLY treatment of breast cancer can be highly effective and can significantly increases long-term survival [1]. Among current clinical and experimental breast-cancer imaging technologies (see, e.g., [2]), the most popular method for breast cancer screening and diagnosis is based on X-ray mammography. In spite of its high resolution, however, X-ray mammography has the following shortcomings [3], [4].

1) It has difficulties detecting breast tumors at their earlier stages.
2) It has a decreased effectiveness in cases of women with dense breasts and has difficulties detecting tumors located near the chest wall or underarm.
3) It has a limited specificity between benign and malignant tissue resulting in high false-alarm rates at clinically accepted detection rates.
4) It uses ionizing radiation.
5) There is a discomfort to patients because of breast compression.

Manuscript received December 30, 2000; revised February 28, 2001. This work was supported in part by the U.S. Environmental Protection Agency under Grant CR-825-225-010, by the National Science Foundation under CAREER Grant ECS-9702195, and by the National Institutes of Health/National Institute of Cancer under Grant 5PO1 CA42745-13.

The authors are with the Department of Electrical and Computer Engineering, Duke University, Durham, NC 27708-0291 USA (e-mail: qhliu@ee.duke.edu).

Publisher Item Identifier S 0018-9480(02)00020-0.

As an alternative and complementary modality for breast imaging, microwave (MW) techniques have been proposed over the last few years [5]–[8] because of its potentially high specificity for breast cancer diagnosis due to the high contrast in electrical properties between normal and malignant human breast tissues.

Due to significantly different sodium concentrations, fluid contents, and electrochemical properties, a significant contrast exists in electrical properties at MW frequencies between the normal and malignant human breast tissues [9]–[13]. For example, at 800 MHz, the relative permittivity (ϵ_r) and electrical conductivity (σ) for normal mammary tissues are around $\epsilon_r \approx$16 and $\sigma \approx$0.16 S/m, respectively, while they are $\epsilon_r \approx$57.2 and $\sigma \approx$1.08 S/m, respectively, for a malignant breast tumor. The contrast is 3.75 for the relative permittivity and 6.75 for the electrical conductivity. This high contrast gives rise to a large electromagnetic scattering signal when electromagnetic waves are applied to a malignant tumor embedded in a normal tissue.

Compared to X-ray mammography, MW mammography has the following potential advantages.

1) The high contrast in electrical properties can potentially provide a high specificity to distinguish between normal and malignant breast tissues. MW mammography may be able to detect, at an earlier stage, small tumors otherwise undetectable by X-ray mammography.
2) Microwave imaging (MWI) utilizes nonionizing radiation for breast cancer imaging. The MW radiation levels required are well within accepted safety standards, and there are no contrast agents involved.
3) The examinations using MWs are well tolerated since no breast compression is required for the patient. The MWI method provides a useful alternative and complement to the diagnostic information provided by X-ray mammography.

During the last decade, there has been significant progress in the development of experimental prototypes of two-dimensional (2-D) and three-dimensional (3-D) MWI systems based on various ideas [5]–[7], [14], [15]. These systems image 2-D (and more recently, 3-D) small- and medium-size objects, and sometimes even the full body [16]–[18]. Substantial research has also been carried out specifically for breast cancer diagnosis with narrow-band [14] and wide-band [5], [6] signals. A recent report, apparently the first clinical experiments, shows very promising results for MW breast imaging [7].

From the practical viewpoint, one of the most significant problems for current MWI systems is their lower spatial

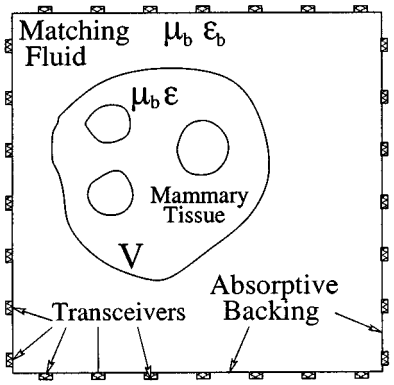

Fig. 1. Typical geometry for forward and inverse problems in MW breast imaging. Transmitting and receiving antennas are mounted on the rim of a fluid-holding box with an absorptive backing.

resolution. There has been great interest in inverse problems for biomedical applications of MWs to improve the resolution [19], [22], [23], [20], [21]. Unlike X-ray imaging techniques, which only need to consider the attenuation of the X-ray, for MWI technology, we need to consider multiple scattering (i.e., diffraction) of MWs within the tissues. This is a significant effect and cannot be neglected [18]. From this viewpoint, the very advantage of high contrast in electrical properties between normal and malignant tissues can also pose a major limitation if not treated correctly. This is because the high contrast introduces large multiple scattering effects, leading to a low resolution if linear or quasi-linear methods are used to invert for the object properties.

In this paper, we develop fast-forward and inverse-scattering algorithms to fully unravel multiple scattering effects. These algorithms are applied to form high-resolution images for an experimental prototype of a MW breast-imaging system recently developed at Duke University, Durham, NC. Our imaging technique uses the fast Fourier transform (FFT), the extended Born approximation (EBA), conjugate and biconjugate gradients, and contrast source-inversion (CSI) methods.

This paper is organized as follows. We briefly present the integral equation for the 2-D TM problem in Section II. The forward and inverse solution methods are presented in Sections III and IV. Numerical results are shown in Section V to demonstrate the efficacy of the technique. Conclusions are presented in Section VI.

II. Integral Equation

In this paper, we focus on 2-D MWI problems. We assume a TM_z wave from a finite source impinging on an inhomogeneous medium with a high contrast in both dielectric constant and conductivity with respect to a homogeneous background medium. In MW breast imaging, a matching material with a nonreflective backing is usually used to eliminate the reflections at the tissue/air interface, as illustrated in Fig. 1. In that case, the background medium is the matching fluid with properties similar to a normal breast tissue.

Fig. 1 illustrates the general scenario of the problem, where an inhomogeneous object with dielectric constant $\epsilon_r(\mathbf{r})$, conductivity $\sigma(\mathbf{r})$, and a constant magnetic permeability μ_b is immersed in a background medium with the corresponding parameters ϵ_{rb}, σ_b, and μ_b. With an implied time dependence of $\exp(j\omega t)$, the complex permittivity for the object and background can be written as $\epsilon = \epsilon_0\epsilon_r - j\sigma/\omega$ and $\epsilon_b = \epsilon_0\epsilon_{rb} - j\sigma_b/\omega$. In the 2-D TM_z case, all field and source variables are only functions of $\mathbf{r} = (x, y)$. For an electric current source $\mathbf{J} = \hat{z}J_z(\mathbf{r})$ in such an inhomogeneous medium, the electric field $\mathbf{E} = \hat{z}E_z(\mathbf{r})$ satisfies the integral equation

$$E_z(\mathbf{r}) = E_z^{\mathrm{inc}}(\mathbf{r}) + \int_D d\mathbf{r}' g(\mathbf{r}-\mathbf{r}')\left[k^2(\mathbf{r}') - k_b^2\right]E_z(\mathbf{r}') \qquad (1)$$

where the complex wavenumbers k and k_b are defined by $k^2 = \omega^2\mu_b\epsilon$ and $k_b^2 = \omega^2\mu_b\epsilon_b$, respectively, and $g(\mathbf{r}-\mathbf{r}') = (1/4j)H_0^{(2)}(k_b|\mathbf{r}-\mathbf{r}'|)$ is the Green's function for a homogeneous background medium. The incident field E_z^{inc} in (1) is the field in the background medium, i.e., in the absence of the scatterer (or $k = k_b$).

Equation (1) is the central equation we use in this paper for both the forward and inverse solutions. In the forward problem, both the medium properties and the domain of inhomogeneity D are known; our aim is to solve (1) to obtain the electric field. In the inverse problem, the electromagnetic fields are measured at some discrete points, usually outside the domain of inhomogeneity; the medium properties (including the domain of inhomogeneity) are unknowns to be determined. However, we assume that the scatterer is finite and, thus, can always be enclosed in a large rectangular region D.

A. Historical Note

There is a large body of literatures dealing with both the forward and inverse solutions for integral equations similar to (1). It is not our purpose to present a thorough review of these works. Here, we will briefly summarize the developments leading to the methods used in this study.

In the context of low-frequency electromagnetic induction applications, the forward and inverse problems were solved with the EBA in [25]–[27]. An FFT accelerated EBA method was developed as fast-forward and inverse solvers in [28], and has been used as a preconditioner for the conjugate-gradient fast Fourier transform (CG–FFT) method in [29], [30], and [45]. However, the application in MWI involves significantly different physics than in our previous low-frequency problems where the wave fields are diffusive because of the dominant conduction current. The dominant wave phenomenon in the MWI application makes both the forward and inverse problems more challenging. The biconjugate-gradient fast Fourier transform (BCG–FFT) method used in this paper is an application of our recent method presented in [49].

III. Forward-Solution Methods

There are two purposes for the forward solution. First, it will be used to simulate and calibrate the imaging system. Secondly, it will be used to test the inverse algorithms by providing the simulated "measured" data. Furthermore, other inverse algorithms (unlike those in this paper) may require repeated forward solutions.

In the forward problem, the unknown electric field E_z appears both on the left-hand side and inside the integrand of (1). The conventional way of solving (1) is the method of moments (MOM), which discretizes the integral equation with N electric field unknowns in terms of basis functions inside D, and solves the resulting matrix equation by direct matrix inversion. Unfortunately, this direct method is prohibitively expensive, costing $O(N^3)$ CPU time and $O(N^2)$ computer memory.

A. EBA

An efficient way to solve (1) is to use the Born approximation [24], i.e., to assume that the electric field inside the integrand in (1) can be approximated by the incident field E_z^{inc}. The total field can then be easily calculated by performing the integral of the Green's function operating on the Born approximated current density.

The Born approximation has a very limited range of validity when the contrast and/or the size of the scatterer is small [25]–[27]. To increase the range of validity, one can use the EBA put forward in [25]. In essence, the EBA makes use of the fact that the Green's function $g(\mathbf{r}-\mathbf{r}')$ is highly peaked (in fact, singular) when $\mathbf{r} \to \mathbf{r}'$, and becomes relatively small for larger $|\mathbf{r}-\mathbf{r}'|$. Hence, one can replace $E_z(\mathbf{r}')$ inside the integrand in (1) with $E_z(\mathbf{r})$ and approximate (1) by

$$E_z^p(\mathbf{r}) \approx E_z^{\text{inc}}(\mathbf{r}) + E_z^p(\mathbf{r}) k_b^2 \int_D d\mathbf{r}' g(\mathbf{r}-\mathbf{r}')\chi(\mathbf{r}'), \qquad \mathbf{r} \in D \tag{2}$$

where $\chi = \left(k^2/k_b^2 - 1\right)$ is the contrast function. Consequently, the electric field in the integrand of (1) can be more accurately approximated by the solution of (2) when this approximated field E_z^p from (2) is substituted into the integrand of (1) to yield

$$E_z^{(\text{EB})}(\mathbf{r}) = E_z^{\text{inc}}(\mathbf{r}) + k_b^2 \int_D d\mathbf{r}' g(\mathbf{r}-\mathbf{r}')\chi(\mathbf{r}')M^{-1}(\mathbf{r}')E_z^{\text{inc}}(\mathbf{r}') \tag{3}$$

where

$$M(\mathbf{r}) = 1 - k_b^2 \int_D d\mathbf{r}' g(\mathbf{r}-\mathbf{r}')\chi(\mathbf{r}'), \qquad \mathbf{r} \in D. \tag{4}$$

It has been shown that the EBA has a significantly larger range of applicability than the Born approximation [25], [26], [28], [29], [30]. Furthermore, the computational cost for (3) remains essentially the same as the Born approximation, i.e., $O(M_f N)$ arithmetic operations, where M_f is the number of field points. However, (4) requires $O(N^2)$ arithmetic operations since $M(\mathbf{r})$ is needed for all N points within the object. Thus, the total cost of the EBA is $O(C_1 M_f N + C_2 N^2)$, where C_1 and C_2 are constants. This is still much more efficient than the direct MOM with $O(N^3)$ arithmetic operations.

B. Using FFT to Speed up the EBA: FFT–EBA Method

We adopt an efficient method for the electromagnetic induction problem [28]–[30] to speed up the EBA computation of the electric field at N points within the scatterer. This method is based on the observation that the integrals in (3) and (4) are convolutional. Hence, by using the convolution theorem, one can solve for the electric field within the EBA approach as

$$\begin{aligned} E_z^{(\text{EB})}(\mathbf{r}) &= E_z^{\text{inc}}(\mathbf{r}) + k_b^2 \mathcal{F}^{-1}\left\{\mathcal{F}\left[g(\mathbf{r})\right]\mathcal{F}\left[\chi(\mathbf{r})M^{-1}(\mathbf{r})E_z^{\text{inc}}(\mathbf{r})\right]\right\} \\ &\equiv \mathcal{L}_{\text{EB}}^{-1}\left[E_z^{\text{inc}}\right] \end{aligned} \tag{5}$$

where $\mathcal{F}$ and $\mathcal{F}^{-1}$ stand for the 2-D forward and inverse Fourier transforms, respectively, which, in their discrete forms with zero-padded arrays, can be achieved efficiently through the FFT algorithms with $O(N \log_2 N)$ arithmetic operations. Equation (5) also defines the operator $\mathcal{L}_{\text{EB}}$.

This improvement reduces the computational cost of the EBA from $O(N^2)$ to $O(N \log_2 N)$. Furthermore, it makes possible the following hybridization of the EBA with the CG–FFT and BCG–FFT methods without increasing the overall cost to $O(N^2)$. For the convenience of the following discussions, we refer to this improved approach as the FFT–EBA method.

C. EBA as a Preconditioner for CG–FFT and BCG–FFT Methods

Although the EBA is more accurate than the Born approximation, its error increases when the object becomes very large in size or in contrast against the background. An efficient full-wave method that, in principle, does not suffer from this limitation is the CG–FFT method [33]–[36]. This iterative method is more efficient than the MOM, as it requires only $O(KN \log_2 N)$ arithmetic operations, where K is the number of CG iterations. In our previous studies of the electromagnetic induction problem [29], [30], we propose to incorporate the EBA to further improve the efficiency of the CG–FFT or BCG–FFT methods [49].

Our aim here is to solve (1) for the unknown electric field E_z within the inhomogeneous region. Noting that the integral in (1) is a 2-D convolution between the Green's function $g(\mathbf{r})$ and induced current source $\chi(\mathbf{r})E_z(\mathbf{r})$, we can invoke the convolution theorem to rewrite (1) in an operator form

$$\mathcal{L}\left[E_z\right] \equiv E_z - k_b^2 \mathcal{F}^{-1}\left\{\mathcal{F}\left[g(\mathbf{r})\right]\mathcal{F}\left[\chi(\mathbf{r})E_z\right]\right\} = E_z^{\text{inc}}. \tag{6}$$

This equation can then be solved iteratively by the CG–FFT method [33], [34], [36].

We apply the EBA as the preconditioner. Hence, instead of solving (6) directly, we solve an equivalent problem

$$\mathcal{L}_{\text{EB}}^{-1}\mathcal{L}E_z = E_z^{(\text{EB})} \tag{7}$$

where the preconditioner is the EBA operator defined in (5). Since the preconditioner $\mathcal{L}_{\text{EB}}^{-1}$ is achieved by the FFT algorithm in (5), this new (7) can again be solved efficiently by the CG–FFT method. With this preconditioning, this scheme converges much faster than the regular CG–FFT method [28], [29]. In reality, we found that even using the EBA preconditioner in only the first step of the conjugate-gradient (CG) method can significantly improve the convergence speed for typical electromagnetic problems. This partial preconditioning avoids the additional cost of the preconditioning in the majority of the

CG steps. The following numerical results are obtained by this preconditioning scheme.

Equation (7) can also be solved by using the biconjugate-gradient (BCG) method [31], [32], [49] with the FFT algorithm. The resulting EBA preconditioned BCG–FFT method is more efficient than the CG–FFT method described above. For procedures of the BCG iterations, see, for example, [31] and [49].

Note that there is no approximation in the above EBA preconditioned CG–FFT and BCG–FFT methods aside from the discretization procedure. The combination of the EBA and CG–FFT and BCG–FFT methods provides a seamless method, which is both efficient and accurate for low- and high-contrast scatterers. In practice, we define an acceptable error criterion $e_{\min}$ based on the L_2-norm residual error

$$e_2 = \frac{||\mathcal{L}E_z - E^{\text{inc}}||}{||E^{\text{inc}}||} \leq e_{\min}$$

to terminate the iteration process. For lower contrast problems, if the initial step of the EBA solution suffices, no further CG or BCG procedures are needed; for higher contrast problems, the CG or BCG iterations will continue until the residual error is smaller that $e_{\min}$. Note that e_2 can always be calculated even though the exact solution is not known. Compared with the regular CG–FFT and BCG–FFT methods, these EBA preconditioned methods are more efficient [29].

IV. Nonlinear Inverse-Scattering Algorithms

In the inverse problem, the unknown material properties $\epsilon_r(\mathbf{r})$ and $\sigma(\mathbf{r})$ are inferred from the scattered electric field measured at some discrete locations. This inverse problem is nonlinear, as the material properties appear both in the contrast function χ and in E_z in (1). Furthermore, this inverse problem is ill posed because of the sparsity of measured data contaminated by noise [38].

Methods for solving the electromagnetic inverse-scattering problem include linear [37] and nonlinear [26], [28], [38], [40], [42], [43], [47], [48] inverse methods. (See [44] for more complete references.) In this study, we apply two methods for nonlinear inverse problems. The first is an improved two-step inversion method based on the EBA [25]–[28], [45]. This is a compromise between the linear and full nonlinear inversion methods. The second nonlinear method is based on the CSI method [46]–[48] with an improved initial solution through the two-step nonlinear inversion.

A. Two-Step Inverse Method Based on EBA

1) FFT Enhanced Two-Step Inversion Method : The EBA in (3) can be rewritten for the scattered field as

$$E_z^{\text{sct}}(\mathbf{r}_R, \mathbf{r}_T) = k_b^2 \int_D d\mathbf{r}'\, g(\mathbf{r}_R - \mathbf{r}')w(\mathbf{r}')E_z^{\text{inc}}(\mathbf{r}', \mathbf{r}_T) \quad (8)$$

where, for clarity, we have explicitly included the transmitter and receiver locations $\mathbf{r}_T$ and $\mathbf{r}_R$ in the electric field. In the above, $w(\mathbf{r})$ is defined as

$$w(\mathbf{r}) = \chi(\mathbf{r})M^{-1}(\mathbf{r}) \quad (9)$$

where M is given in (4).

The two-step linear inverse method has been applied in [27] and enhanced by the FFT algorithm [28]. Here, we summarize this FFT enhanced version adapted to the current problem in Cartesian coordinates [30] as follows.

Step 1) **The induced source:** The first step of this scheme is to invert for the induced source function $w(\mathbf{r})$ from (8). With the trapezoidal rule, (8) can be discretized into a linear system of equations

$$\mathbf{A} \cdot \mathbf{w} = \mathbf{d} \quad (10)$$

where $\mathbf{A}$ is an $M \times N$ matrix, $\mathbf{d}$ is the data vector containing the measured scattered field, N is the number of unknowns in domain D, and $M = M_R M_T$ is the number of measured data points determined by the number of source locations M_T and the number of receiver locations M_R. Note that this equation for the unknown $\mathbf{w}$ is a classical linear ill-posed problem. A minimum-norm solution to (10) can be obtained by an optimization procedure. That is, we find a solution $\mathbf{w}$ that will minimize the L_2 norm functional

$$I = ||\mathbf{d} - \mathbf{A} \cdot \mathbf{w}||^2 + \gamma||\mathbf{w}||^2 \quad (11)$$

where γ is a regularization parameter. Minimizing I yields a linear equation as follows:

$$(\mathbf{A}^\dagger \cdot \mathbf{A} + \gamma\mathbf{I})\mathbf{w} = \mathbf{A}^\dagger \cdot \mathbf{d}. \quad (12)$$

Equation (12) can be solved iteratively by the CG procedure with the cost of $O(MN)$ per iteration.

Step 2) **The contrast function:** Once $w(\mathbf{r})$ is obtained, our second linear inversion step is to invert for $\chi(\mathbf{r})$ (and, thus, $\epsilon_r(\mathbf{r})$ and $\sigma(\mathbf{r})$) using (9) and (4). That is to solve the following equation:

$$\chi(\mathbf{r}) + k_b^2 w(\mathbf{r}) \cdot \mathcal{F}^{-1}\Big\{\mathcal{F}[g]\mathcal{F}\big[\chi(\mathbf{r})\big]\Big\} = w(\mathbf{r}). \quad (13)$$

Equation (13) is a linear equation for the unknown contrast function $\chi(\mathbf{r})$, a function representing the difference between the anomaly and background. Equation (13) is a well-posed linear problem. It can be solved iteratively by using the CG method to find unknown complex permittivity $\epsilon = \epsilon_0\epsilon_r - j\sigma/\omega$. In the CG procedure, the Green's function operations are accelerated by the FFT algorithm. This represents an acceleration over the earlier versions of the two-step inversion scheme [26], [27], and reduces the number of arithmetic operations to $O(N \log_2 N)$ in each CG iteration [28], [30].

With these procedures, the original nonlinear inverse problem has been converted into two linear inverse problems based on the EBA. This scheme uses the FFT algorithm to accelerate the second linear inversion step to greatly reduce the computational cost from $O(N^3)$ to $O(N \log_2 N)$, where N is the number of unknown pixels in the inverse model. Next, we will improve the memory efficiency in the first linear inversion step.

2) Improved Two-Step Inversion Scheme: The above two-step inversion scheme is a significantly enhanced version of earlier work since the total CPU time is reduced to $O(C_1K_1MN + C_2K_2N\log_2 N)$, where C_1 and C_2 are constants, and K_1 and K_2 are the numbers of the CG iterations in the two steps, respectively [28]. However, the memory requirement is still large for the first step as $\mathbf{A}$ requires $O(MN)$ storage. We can further improve the memory requirement in a way similar to the CSI method [47], [48]. Defining S and D as the domain of measured data and the imaged domain, respectively, and Green's operator G_S and G_D as

$$G_{S,D}[\cdot] = k_b^2 \int_D d\mathbf{r}' g(\mathbf{r}-\mathbf{r}')[\cdot], \qquad \mathbf{r} \in S \text{ or } D \tag{14}$$

we can rewrite (8) as

$$E_z^{\text{sct}}(\mathbf{r}_R, \mathbf{r}_T) = \left\{ G_S\left[E_z^{\text{inc}}(\mathbf{r}', \mathbf{r}_T) w(\mathbf{r}')\right] \right\}(\mathbf{r}_R). \tag{15}$$

The first step of the EBA inversion for $w(\mathbf{r})$ can then be stated as the minimization of the functional

$$F = \left\| E_z^{\text{sct}} - G_S\left[E_z^{\text{inc}} w\right] \right\|_S^2 + \gamma \|w\|_D^2 \tag{16}$$

where S is the measured data domain. This functional is basically the same as that in (11), except that it is in an undiscretized form.

Since (16) is a quadratic functional of w, it can be minimized by the conjugate gradient procedure. Defining the data error

$$\rho_j = E_{zj}^{\text{sct}} - G_S\left[E_{zj}^{\text{inc}} w\right]$$

we can update w_n by the following CG procedure:

$$w_n = w_{n-1} + \alpha_n v_n \tag{17}$$

where the update directions $\{v_n\}$ are chosen by the Polak–Ribiére CG directions

$$v_0 = 0 \tag{18}$$

$$v_n = d_n + \frac{\langle d_n, d_n - d_{n-1}\rangle_D}{\langle d_{n-1}, d_{n-1}\rangle_D} v_{n-1}, \qquad n \geq 1. \tag{19}$$

The gradient (Frechet derivative) of the cost functional with respect to w is given by

$$d_n = -k_b^{*2} \sum_{j=1}^{M_T} \left[E_z^{\text{inc}}(\mathbf{r}, \mathbf{r}_{T,j})\right]^* \int_S g^*(\mathbf{r}-\mathbf{r}') \rho_{j,n-1}(\mathbf{r}') d\mathbf{r}' + \gamma w_{n-1}, \quad \mathbf{r} \in D. \tag{20}$$

where the asterisk denotes the complex conjugate. By minimizing F in (16), the constant α_n is determined as

$$\alpha_n = -\frac{\langle d_n, v_n\rangle_D}{\left\| G_S\left[E_z^{\text{inc}} v_n\right] \right\|_S^2 + \gamma \|v_n\|_D^2}. \tag{21}$$

Note that an important difference between this procedure and that in the CSI (see [47]) is that w in (16), unlike the contrast source in CSI, is not a function of source location. Therefore, the inversion is much faster than the CSI because the system of equations for w is much smaller.

Note that even though the CPU time for this modified first step remains $O(K_1MN)$, the computer memory cost is reduced from $O(MN)$ to $O(M_TN)$, where $M = M_TM_R$ is the number of measured data. After w is obtained, we solve (13) to determine the complex permittivity profile with the computational complexity $O(N\log_2 N)$.

B. EBA Preconditioned CSI

For many problems, the two-step inversion scheme provides satisfactory results. However, since the EBA is an approximate method, the inverse procedure based on the EBA to reconstruct the complex permittivity profile may not always be adequate, especially for very high contrasts. Under those circumstances, some nonlinear inversion methods can be employed to achieve better results. The recently developed CSI method has an important feature in that it does not require a forward solution in the inverse iterations [47], [48]. We adopt this CSI method for MW breast imaging by defining an object functional

$$F = \eta_S \sum_j \left\| E_z^{\text{sct}} - G_S[w_j] \right\|_S^2 + \eta_D \sum_j \left\| \chi E_z^{\text{inc}} - w_j + \chi G_D[w_j] \right\|_D^2 \tag{22}$$

where $w_j = \chi(\mathbf{r}) E_z(\mathbf{r}, \mathbf{r}_{T,j})$ for $\mathbf{r} \in D$ is the contrast source, and the normalization constants η_S and η_D are chosen so that both terms in (22) are equal to one if $w_j = 0$. The procedures to minimize F in (22) for the solution of χ can be found in [48]. It is worth noting that even though (22) is similar to (16), the minimization of (22) is more time consuming since, here, w_j is a function of the source location.

Given the measured scattered electric field, we can invert for the permittivity profile by the CSI method. However, in contrast to the earlier CSI implementations, we use the above two-step inversion result rather than the back-propagation as the initial solution to speed up the convergence. Preliminary results show that this improved CSI procedure accelerates the convergence of the inversion as the two-step EBA inversion already achieves a reasonable approximation. For our typical examples, the EBA preconditioned CSI method requires less than half of the iterations and CPU time of the original CSI method.

V. Numerical Results and Discussions

Our numerical models will aim to simulate a prototype MWI system for breast cancer imaging developed at Duke University. Fig. 1 schematically shows the basic geometry modeled in this study. The rectangular cylinder is filled with a matching fluid whose electrical properties are close to those of the normal breast tissue. The outer rim of the cylinder is an absorptive material to attenuate outgoing waves. This configuration is aimed to eliminate reflections from the tissue/ambiance interface and the cylinder/air interface in order to enhance the image resolution. An array of transmitting and receiving MW antennas are mounted on the outer surface of the cylinder. The operating frequency for the following examples is 800 MHz (except as oth-

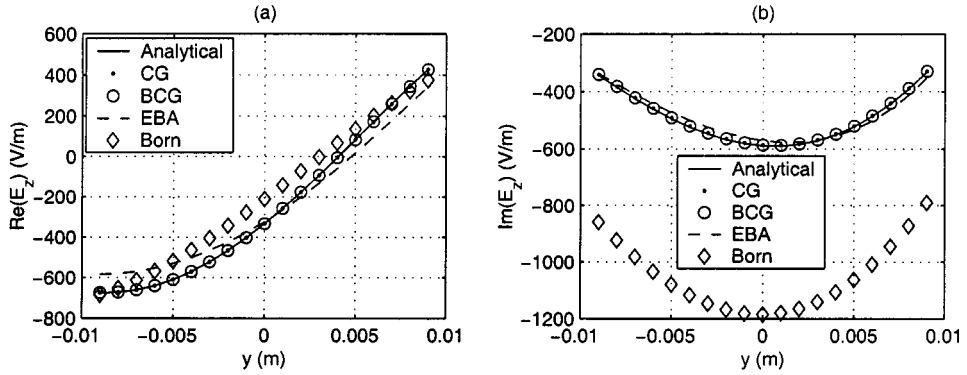

Fig. 2. Comparison of the EBA, Born, CG–FFT, and BCG–FFT methods and analytical solution for a circular cylinder ($\epsilon_r = 64$, $\sigma = 0.64$ S/m) with the center at the origin. The line source is at $(0, 0.03)$ m, while the receivers are at $(0, y)$ m, $y \in (-0.01, 0.01)$ m.

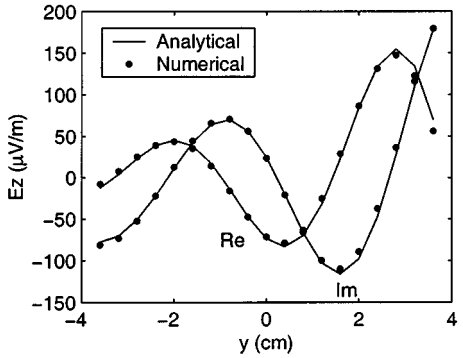

Fig. 3. Lossy cylinder with $\epsilon_r = 57.2$, $\sigma = 1.08$ S/m, and diameter 0.08 m. The line source is at $(0, 0.08)$m, while the receivers are at $(0, y), y \in (-0.04, 0.04)$.

erwise indicated), although both the apparatus and numerical models are designed for wide-band signals.

A. Forward-Modeling Results

In our 2-D forward model, we simulate an electric current source $\mathbf{J} = \hat{z}J_z(x, y)$ in an inhomogeneous conductive medium with dielectric constant $\epsilon_r(x, y)$, conductivity $\sigma(x, y)$, and constant permeability μ_0. The background medium is homogeneous and has the properties $\epsilon_{rb} = 16$, $\sigma_b = 0.16$ S/m, and $\mu_b = \mu_0$ to simulate the normal tissue and the matching fluid inside the cylinder.

We first study the accuracy of the EBA method against the Born approximation, CG–FFT, BCG–FFT, and analytical solution for a circular tumor with $\epsilon_r = 64$, $\sigma = 0.64$ S/m and a diameter of 0.01 m. The line source is 0.03 m away from the cylinder center. Fig. 2 shows that the EBA result has a much greater accuracy than the Born approximation for this high contrast medium. Both CG–FFT and BCG–FFT results have the same accuracy, and take four and three iterations to reach a relative residual error of 0.01% with the EBA preconditioner. The CPU time for the Born approximation, EBA, CG–FFT, and BCG–FFT methods are 1.2, 1.2, 3.5, and 2.2 s, respectively, on a SUN Ultra 60 Workstation.

For larger contrasts and higher frequencies, as expected, the accuracy of the EBA will decrease, and full-wave CG- and BCG–FFT methods have to be used. In the second example, we simulate a large-contrast circular cylinder with $\epsilon_r = 57.2$, $\sigma = 1.08$ S/m, and a diameter of 0.08 m. The line source is 0.12 m away from the center of the cylinder. We compute the electric field inside the cylinder by the CG–FFT and analytical solution. Fig. 3 is the comparison of the numerical result and analytical solution. We observe that both real and imaginary parts of the numerical result agree well with the analytical solution.

Fig. 4 compares the CG–FFT and BCG–FFT results for a tissue with multiple tumors. The results again show excellent agreement between these two methods. The BCG–FFT method converges in only two iterations, while the CG–FFT method converges in eight iterations to a residual error of 0.01%. The CPU time for this case is 4.5 s, and 2.2 s for the CG–FFT and BCG–FFT methods, respectively.

B. Inverse-Scattering Results

For the image formation, we have developed the two-step inverse method that is based on the EBA and CSI method. The EBA inversion aims to produce a fast, albeit quantitatively less accurate, image while the CSI method aims to produce an excellent accuracy at the expense of more computational cost. The two-step inversion result is used as the preconditioner for the CSI result. In the following examples, the measured data is obtained by the CG–FFT method with a much finer grid than that used in the inversion. Neither the EBA, nor the CSI method requires a forward solution during the inversion iterations, thus, the so-called "inverse crime" is not committed here. The background is the normal tissue with properties given for Fig. 2. We use 60 transmitters and 60 receivers uniformly distributed on the four edges of a square of size 16×16 cm^2, giving a total of 3600 measured data points. The region to be inverted is divided into 29×29 unknown pixels with a cell size 0.0052×0.0052 m^2.

In the first example, there are two anomalous objects within the homogeneous medium. The first anomaly has a dielectric constant of $\epsilon_r = 40$ and conductivity $\sigma = 1.08$ S/m. The other object has $\epsilon_r = 57.2$, $\sigma = 1.08$ S/m. These two anomalies simulate two tumors; the first one perhaps in the process of becoming malignant, while the second one is malignant. There is a significant difference in the electrical properties of these two tumors. The reconstructed results are shown in Fig. 5. Both the permittivity and conductivity anomalies are well resolved. In

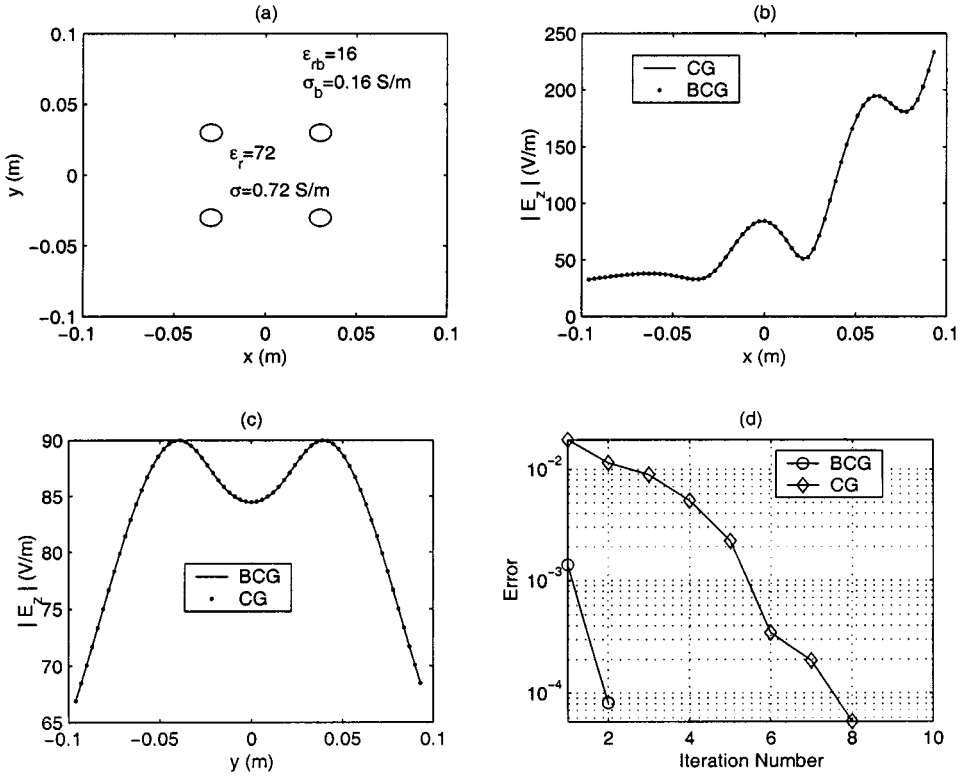

Fig. 4. CG–FFT and BCG–FFT results for a tissue with multiple tumors. The line source is located at $(0, -0.189)$. (a) Geometry of four tumors ($\epsilon_r = 72$, $\sigma = 0.72$ S/m) in a background medium ($\epsilon_{rb} = 16$, $\sigma_b = 0.16$ S/m). (b) Magnitude of electric field along $(x, 0), x \in (-0.1, 0.1)$ and (c) along $(0, y), y \in (-0.1, 0.1)$. (d) Convergence curves for the CG–FFT and BCG–FFT methods.

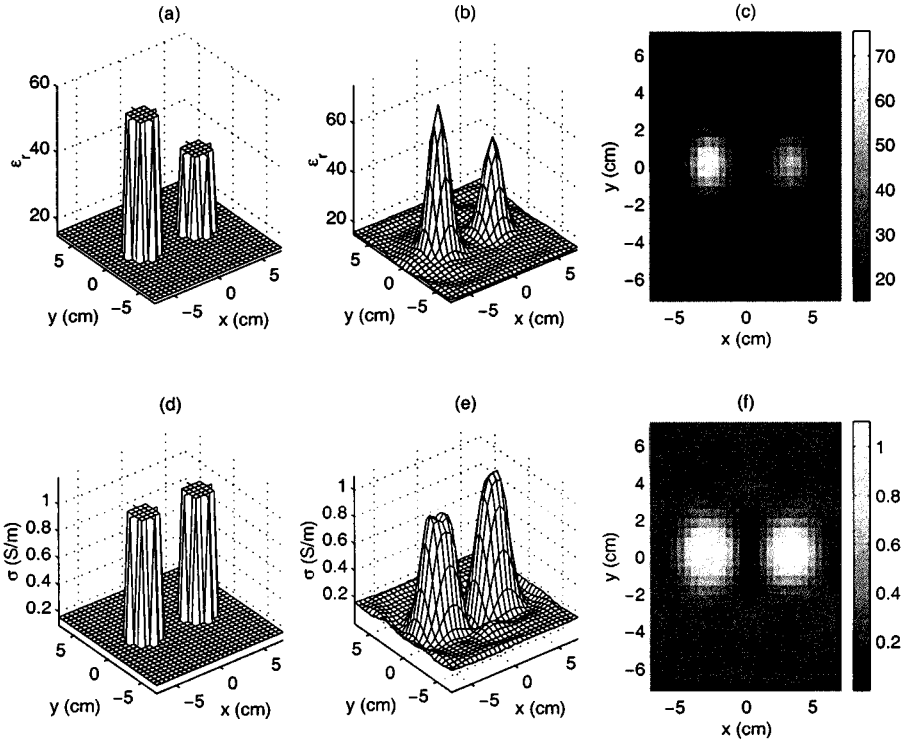

Fig. 5. Simultaneous inversion of dielectric constant and conductivity profiles at 800 MHz. The ground truth of: (a) ϵ_r and (d) σ profiles. Inverted dielectric: (b), (c) constant and (e), (f) conductivity.

this case, the preconditioned CSI method takes 70 iterations, and 8 min and 7 s CPU time to converge to a relative residual error of 0.97%.

We then demonstrate the super resolution [38], [39] of the nonlinear inverse-scattering CSI algorithm. The same measurement geometry as in Fig. 5 is used. We use an EBA precondi-

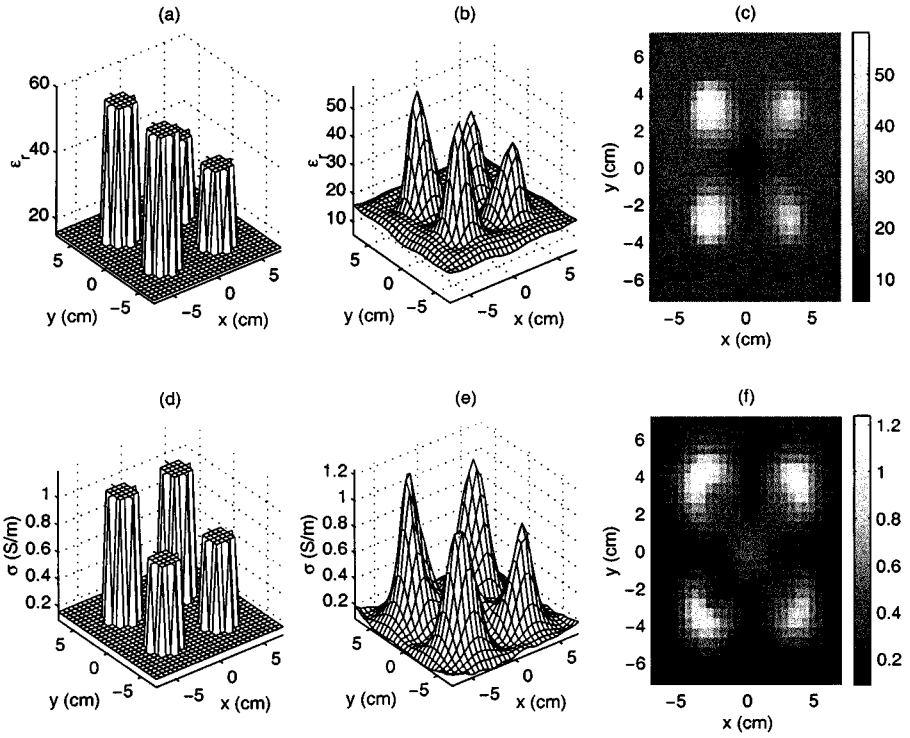

Fig. 6. Super resolution of dielectric constant and conductivity anomalies separated by only 0.22 wavelengths at 800 MHz. The ground truth of: (a) ϵ_r and (d) σ profiles. The inverted dielectric: (b), (c) constant and (e), (f) conductivity. The measured data $E_z^{\rm sct}$ has a 10% Gaussian noise ($\mathrm{SNR} = 20$ dB).

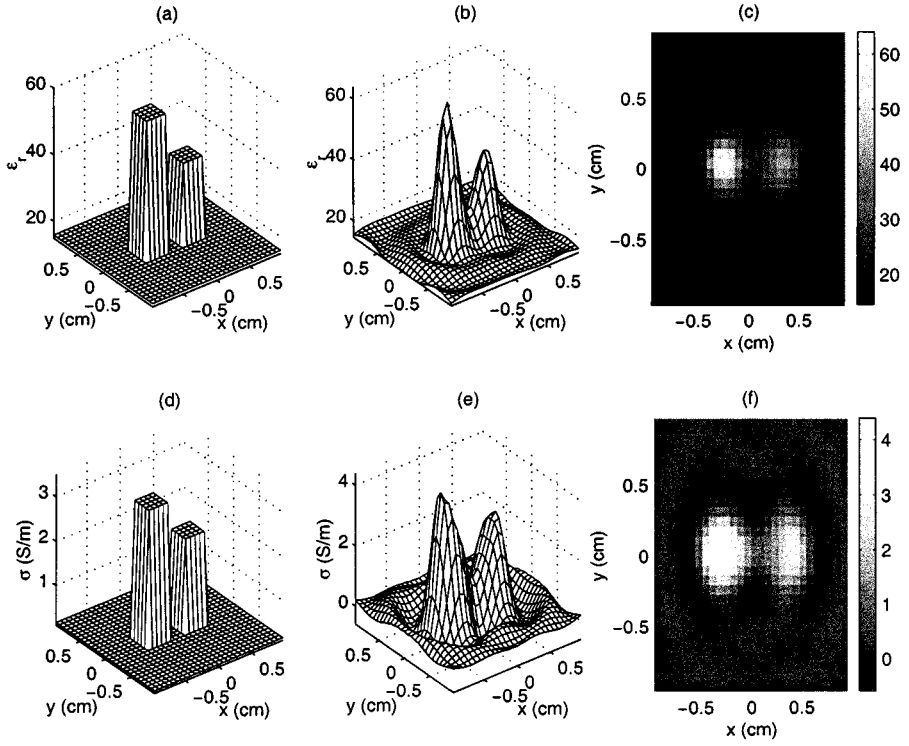

Fig. 7. Inversion of dielectric constant and conductivity anomalies separated by only 0.22 wavelengths at 6 GHz with properties as in Fig. 5. The ground truth of: (a) ϵ_r and (d) σ profiles. The inverted dielectric: (b), (c) constant and (e), (f) conductivity.

tioned CG–FFT to simulate the electric field outside the inversion area. Within the region being inverted, there are four anomalies separated only by 0.22 wavelengths (2.06 cm) at 800 MHz. We add 10% Gaussian noise to the scattered field data (i.e., signal-to-noise ratio $\mathrm{SNR} = 20$ dB). Fig. 6 shows the ground truth and reconstructed profiles. This example clearly demonstrates that the so-called super resolution [38] can be achieved for the high-contrast medium in MW breast imaging. This super resolution is possible because the nonlinear multiple scattering has been fully accounted for and because of the near-field mea-

surement. For more in-depth discussions on this topic, the reader is referred to [38] and [39].

Finally, we study the potential resolution at a higher frequency of 6 GHz. In this case, we invert for two very small anomalies only 0.28 cm apart and complex permittivity the same as in Fig. 5. The image area is about 2×2 cm^2 with 29×29 pixels, giving a comparable computational cost as Figs. 5 and 6. RMS noise of 10% for the scattered field data has been added. Fig. 7 shows that our inverse algorithm can resolve these small objects when operated at a high frequency.

C. Discussions

This study represents a new application of some of our recent fast algorithms developed for low-frequency electromagnetic subsurface sensing problems [28]–[30], [35], [41], [45], [49]. However, for low-frequency induction problems, the conduction current is dominant and only the conductivity profile can be inverted. For MWI, both dielectric constant and conductivity profiles must be inverted simultaneously. This represents a much more difficult problem, and an increasingly important application in biomedical imaging.

The above numerical results show the efficacy of our 2-D forward- and inverse-scattering methods. In spite of this, there are many outstanding issues that require further research. Firstly, it would have been ideal if there is experimental verification. However, at present, we are unable to present this verification because our experimental setup has 3-D waveguide aperture transmitting antennas, which cannot be adequately modeled by our 2-D methods. Secondly, 3-D effects in breast tumor detection are expected to be very strong. Therefore, we are currently pursuing a better experimental verification in the following two directions: we are modifying our experimental setup so that it can be better modeled by our 2-D models with some 3-D compensation techniques, and we are developing full 3-D forward- and inverse-scattering methods to include all 3-D effects in MWI measurements. Thirdly, the breast tissue is not homogeneous because of the presence of fat, glandular tissue, etc. This inhomogeneity will definitely degrade the images. These important issues will be addressed in our future research.

VI. Conclusions

We have applied fast-forward and inverse methods to simulate 2-D MWI for breast tumor detection. The forward methods are based on the EBA, FFT, and CG and BCG methods. The FFT algorithm is used to expedite the EBA calculation, while the EBA is used to precondition the CG–FFT and BCG–FFT methods. The combination of these basic ingredients results in algorithms with a complexity of $O(N \log_2 N)$. The inverse methods are based on a two-step nonlinear inversion and the CSI methods, which do not require forward solutions during the iterations of the inverse solution. Numerical results demonstrate the efficiency of the forward and inverse methods, and the high resolution of the image-formation algorithm for the breast-imaging applications. Future work includes experimental validation and 3-D algorithms.

References

[1] J. R. Harris, M. E. Lippman, U. Veronesi, and W. Willett, "Medical progress: Breast cancer," *New Eng. J. Med.*, vol. 327, no. 5, pp. 319–328, 1992.

[2] M. Douek, T. Davidson, and I. Taylor, "Breast cancer imaging—What are the optimal modalities?," *Eur. J. Surg. Oncol.*, vol. 24, no. 6, pp. 573–382, 1998.

[3] F. M. Hall, J. M. Storella, D. Z. Silverstone, and G. Wyshak, "Non-palpable breast-lesions: Recommendation for biopsy based on suspicion of carcinoma at mammography," *Radiology*, vol. 167, no. 2, pp. 353–358, 1988.

[4] C. Boetes, R. D. M. Mus, R. Holland, J. O. Barentsz, S. P. Strijk, T. Wobbes, J. H. C. Hendriks, and S. H. J. Ruys, "Breast tumors: Comparative accuracy of MR imaging relative to mammography and US for demonstrating extent," *Radiology*, vol. 197, no. 3, pp. 743–747, 1995.

[5] S. C. Hagness, A. Taflove, and J. E. Bridges, "Two-dimensional FDTD analysis of a pulsed microwave confocal system for breast cancer detection: Fixed-focus and antenna-array sensors," *IEEE Trans. Biomed. Eng.*, vol. 45, pp. 1470–1479, Dec. 1998.

[6] ——, "Three-dimensional FDTD analysis of a pulsed microwave confocal system for breast cancer detection: Design of an antenna-array element," *IEEE Trans. Antennas Propagat.*, vol. 47, pp. 783–791, May 1999.

[7] P. M. Meaney, M. W. Fanning, D. Li, P. Poplack, and K. D. Paulsen, "A clinical prototype for active microwave imaging of the breast," *IEEE Trans. Microwave Theory Tech.*, vol. 48, pp. 1841–1853, Nov. 2000.

[8] E. C. Fear and M. A. Stuchly, "Microwave detection of breast cancer," *IEEE Trans. Microwave Theory Tech.*, vol. 48, pp. 1854–1863, Nov. 2000.

[9] R. Pethig, "Dielectric properties of biological materials," *IEEE Trans. Elect. Insulation*, vol. EI-19, pp. 17–20, Jan. 1984.

[10] S. S. Chaudhary, R. K. Mishra, A. Swarup, and J. M. Thomas, "Dielectric properties of normal and malignant human breast tissues at radiowave and microwave frequencies," *Indian J. Biochem. Biophys.*, vol. 21, pp. 76–79, 1984.

[11] W. T. Joines, "Frequency dependent absorption of electromagnetic energy in biological tissue," *IEEE Trans. Biomed. Eng.*, vol. BME-31, pp. 215–222, MONTH 1984.

[12] W. T. Joines, Y. Zhang, C. Li, and R. L. Jirtle, "The measured electrical properties of normal and malignant human tissues from 50 to 900 MHz," *Med. Phys. J.*, vol. 21, no. 4, pp. 547–550, 1994.

[13] A. M. Campbell and D. V. Land, "Dielectric properties of female human breast tissue measured at 3.2 GHz," *Phys. Med. Biol.*, vol. 37, no. 1, pp. 193–210, 1992.

[14] P. M. Meaney, K. D. Paulsen, A. Hartov, and R. K. Crane, "An active microwave imaging system for reconstruction of 2-D electrical property distributions," *IEEE Trans. Biomed. Eng.*, vol. 42, pp. 1017–1025, Oct. 1995.

[15] L. Jofre, M. S. Hawley, A. Broquetas, E. d. l. Reyes, M. Ferrando, and A. R. Elias-Fuste, "Medical imaging with a microwave tomographic scanner," *IEEE Trans. Biomed. Eng.*, vol. 37, pp. 303–312, Mar. 1990.

[16] S. Caorsi, A. Frattoni, G. L. Gragnani, E. Nortino, and M. Pastorino, "Numerical algorithm for dielectric-permittivity microwave imaging of inhomogeneous biological bodies," *Med. Biol. Eng. Comput.*, vol. 29, no. 6, pp. 37–44, 1991.

[17] S. Caorsi, G. L. Gragnani, and M. Pastorino, "An electromagnetic imaging approach using a multi-illumination technique," *IEEE Trans. Biomed. Eng.*, vol. 41, pp. 406–409, Apr. 1994.

[18] S. Y. Semenov, R. H. Svenson, and A. E. Boulyshev *et al.*, "Three-dimensional microwave tomography: Experimental prototype of the system and vector Born reconstruction method," *IEEE Trans. Biomed. Eng.*, vol. 46, pp. 937–946, Aug. 1999.

[19] K. Belkebir, R. E. Kleinman, and C. Pichot, "Microwave imaging-location and shape reconstruction from multifrequency scattering data," *IEEE Trans. Microwave Theory Tech.*, vol. 45, pp. 469–476, Apr. 1997.

[20] O. M. Bucci and T. Isernia, "Electromagnetic inverse scattering: Retrievable information and measurement strategies," *Radio Sci.*, vol. 32, no. 6, pp. 2123–2137, 1997.

[21] S. Caorsi and G. L. Gragnani, "Inverse scattering method for dielectric objects based on the reconstruction of the nonmeasurable equivalent current density," *Radio Sci.*, vol. 34, no. 1, pp. 1–8, 1999.

[22] M. Pastorino, "Short-range microwave inverse scattering techniques for image reconstruction and applications," *IEEE Trans. Instrum. Meas.*, vol. 47, pp. 1419–1427, Dec. 1998.

[23] S. Y. Semenov, A. E. Bulyshev, and A. E. Souvorov *et al.*, "Three-dimensional microwave tomography: Experimental imaging of phantoms and biological objects," *IEEE Trans. Microwave Theory Tech.*, vol. 48, pp. 1071–1074, June 2000.

[24] M. Born and E. Wolf, *Principles of Optics*. New York: Pergamon, 1980.
[25] T. M. Habashy, R. W. Groom, and B. R. Spies, "Beyond the Born and Rytov Approximations. A Nonlinear Approach to Electromagnetic Scattering," *J. Geoph. Res.*, vol. 98, pp. 1759–1775, 1993.
[26] C. Torres-Verdin and T. M. Habashy, "Rapid 2.5-D forward modeling and inversion via a new nonlinear scattering approximation," *Radio Sci.*, vol. 29, pp. 1051–1079, 1994.
[27] ——, "A two-step linear inversion of two-dimensional electrical conductivity," *IEEE Trans. Antennas Propagat.*, vol. 43, pp. 405–415, Apr. 1995.
[28] Z. Q. Zhang and Q. H. Liu, "Reconstruction of axisymmetric media with an FFHT enhanced extended Born approximation," *Inverse Problems*, vol. 16, no. 5, pp. 1281–1296, 2000.
[29] ——, "The hybrid extended Born approximation and CG-FFHT method for axisymmetric media," in *IEEE AP-S Int. Symp. Dig.*, vol. 2, 2000, pp. 602–605.
[30] ——, "Two nonlinear inverse methods for electromagnetic induction measurements," *IEEE Trans. Geosci. Remote Sensing*, vol. 39, pp. 1331–1339, June 2001.
[31] C. F. Smith, A. F. Peterson, and R. Mittra, "The biconjugate gradient method for electromagnetic scattering," *IEEE Trans. Antennas Propagat.*, vol. 38, pp. 938–940, June 1990.
[32] H. Gan and W. C. Chew, "A discrete BCG–FFT algorithm for solving 3D inhomogeneous scatterer problems," *J. Electromag. Waves Applicat.*, vol. 9, pp. 1339–1357, 1995.
[33] D. T. Borup and O. P. Gandhi, "Fast-Fourier-transform method for calculation of SAR distributions in finely discretized inhomogeneous models of biological bodies," *IEEE Trans. Microwave Theory Tech.*, vol. MTT-32, pp. 355–360, Apr. 1984.
[34] A. P. M. Zwamborn and P. M. v. d. Berg, "A weak form of the conjugate gradient FFT method for two-dimensional TE scattering problems," *IEEE Trans. Antennas Propagat.*, vol. 39, pp. 953–960, June 1991.
[35] Q. H. Liu and W. C. Chew, "Applications of the CG–FFHT method with an improved FHT algorithm," *Radio Sci.*, vol. 29, no. 4, pp. 1009–1022, 1994.
[36] M. F. Catedra, R. P. Torres, J. Basterrechea, and E. Gago, *The CG–FFT Method: Application of Signal Processing Techniques to Electromagnetics*. Norwell, MA: Artech House, 1995.
[37] A. J. Devaney, "A filtered backpropagation algorithm for diffraction tomography," *Ultrason. Imaging*, vol. 4, pp. 336–350, 1982.
[38] W. C. Chew and Y. M. Wang, "Reconstruction of the two-dimensional permittivity using the distorted Born iterative method," *IEEE Trans. Med. Imag.*, vol. 9, pp. 218–255, June 1990.
[39] F.-C. Chen, F. C. Chen, and W.C. Chew, "Experimental verification of super-resolution in nonlinear inverse scattering," *Appl. Phys. Lett*, vol. 72, pp. 3080–3082, 1998.
[40] N. Joachimowicz, C. Pichot, and J. Hugonin, "Inverse scattering: An iterative numerical method for electromagnetic imaging," *IEEE Trans. Antennas Propagat.*, vol. 39, pp. 1742–1752, Dec. 1991.
[41] W. C. Chew and Q. H. Liu, "Inversion of induction tool measurements using the distorted Born iterative method and CG-FFHT," *IEEE Trans. Geosci. Remote Sensing*, vol. 32, pp. 878–884, July 1994.
[42] Q. H. Liu, "Reconstruction of two-dimensional axisymmetric inhomogeneous media," *IEEE Trans. Geosci. Remote Sensing*, vol. 31, pp. 587–594, May 1993.
[43] ——, "Nonlinear inversion of electrode-type resistivity measurements," *IEEE Trans. Geosci. Remote Sensing*, vol. 32, pp. 499–507, May 1994.
[44] T. A. Maniatis, K. S. Nikita, and N. K. Uzunoglu, "Two-dimensional dielectric profile reconstruction based on spectral-domain moment method and nonlinear optimization," *IEEE Trans. Microwave Theory Tech.*, vol. 48, pp. 1831–1840, Nov. 2000.
[45] Q. H. Liu, Z. Q. Zhang, and X. M. Xu, "The hybrid extended Born approximation and CG–FFT method for electromagnetic induction problems," *IEEE Trans. Geosci. Remote Sensing*, vol. 39, pp. 347–355, Mar. 2001.
[46] P. M. v. d. Berg and R. E. Kleinman, "A total variation enhanced modified gradient algorithm for profile reconstruction," *Inverse Problems*, vol. 11, pp. L5–L10, 1995.
[47] ——, "A contrast source inversion method," *Inverse Problems*, vol. 13, pp. 1607–1620, 1997.
[48] ——, "Extended contrast source inversion," *Inverse Problems*, vol. 15, pp. 1325–1344, 1999.
[49] Z. Q. Zhang and Q. H. Liu, "Three-dimensional weak-form conjugate- and biconjugate-gradient FFT methods for volume integral equations," *Microwave Opt. Technol. Lett.*, vol. 29, pp. 350–356, June 2001.

Qing Huo Liu (S'88–M'89–SM'94) received the Ph.D. degree in electrical engineering from the University of Illinois at Urbana-Champaign, in 1989.

From September 1986 to December 1988, he was a Research Assistant with the Electromagnetics Laboratory, University of Illinois at Urbana-Champaign, and from January 1989 to February 1990, he was a Post-Doctoral Research Associate. From 1990 to 1995, he was a Research Scientist and Program Leader with Schlumberger-Doll Research, Ridgefield, CT. From 1996 to May 1999, he was with New Mexico State University. Since June 1999, he has been an Associate Professor of Electrical Engineering, Duke University, Durham, NC. He has authored or co-authored over 170 papers in refereed journals and conference proceedings. His research interests include computational electromagnetics and acoustics, biomedical imaging, geophysical subsurface sensing, and inverse problems.

Dr. Liu is a member of Phi Kappa Phi, Tau Beta Pi, and the Society of Exploration Geophysicists (SEG). He is a full member of the U.S. National Committee of URSI Commissions B and F. He currently serves as an associate editor for the IEEE TRANSACTIONS ON GEOSCIENCE AND REMOTE SENSING, for which he also served as a guest editor for the Special Issue on Computational Methods. He was the recipient of the 1996 Presidential Early Career Award for Scientists and Engineers (PECASE) presented by the National Science and Technology Council, the 1996 Early Career Research Award presented by the Environmental Protection Agency, and the 1997 CAREER Award presented by the National Science Foundation.

Zhong Qing Zhang (M'01–SM'01) was born in Henan, China, on October 3, 1966. He received the B.S., M.S., and the Ph.D. degrees from the University of Petroleum, Shandong, China, in 1988, 1991, and 1997, respectively, all in geophysics.

From April 1991 to August 1994, he was a Research Engineer with the Zhongyuan Well Logging Company, Puyang, China. From July 1997 to December 1998, he was with the University of Petroleum, Dongying, China, where he taught advanced graduate electromagnetics and performed research. From January 1999 to May 1999, he was a Post-Doctoral Research Associate at the New Mexico State University. Since June 1999, he has been with the Department of Electrical and Computer Engineering, Duke University, Durham, NC, first as a Post-Doctoral Research Associate and then as a Research Scientist. His current research interests are in fast algorithms for electromagnetic modeling, inverse problems, borehole geophysics, cross-well problems, simulation of integrated circuits, and MWI for biomedical applications.

Tonghui T. Wang received the B.Sc. degree in mathematics from University of Northwestern, Xi'an, China, in 1982, and the M.Sc. degree and Ph.D. degrees in statistics from the University of Windsor, Windsor, ON, Canada, in 1988 and 1992, respectively.

He is currently an Associate Professor in the Department of Electrical and Computer Engineering, New Mexico State University, Las Cruces.

J. A. Bryan, photograph and biography not available at time of publication.

Gary A. Ybarra (S'86–M'86) was born in Hampton, VA, on May 13, 1960. He received the B.S., M.S., and Ph.D. degrees from North Carolina State University, Raleigh, in 1983, 1986, and 1992 respectively, all in electrical and computer engineering.

He is currently an Associate Professor of the Practice and Director of Undergraduate Studies in the Department of Electrical and Computer Engineering, Duke University, Durham, NC. His research interests include radar signal processing and MWI.

Loren W. Nolte (S'56–M'57–LM'99–LSM'01) was born in Napoleon, OH. He received the B.S.E.E. degree from Northwestern University, Evanston, IL, and the M.S.E. and Ph.D. degrees in electrical engineering from The University of Michigan at Ann Arbor, respectively.

Following a year of post-doctoral research in signal detection theory at The University of Michigan at Ann Arbor, he joined the faculty at Duke University, Durham, NC, in 1966, as an Assistant Professor of electrical engineering and became a Professor of electrical and biomedical engineering in 1972. He has held Visiting Professorships at the University of Colorado, Boulder, Colorado State University, Fort Collins, the University of Washington, Seattle, and the Scripps Institution of Oceanography, La Jolla, CA. He is currently Chairman of the Department of Electrical and Computer Engineering, Duke University. His research interests have included optimal Bayesian approaches to adaptive detection, classification, tracking and localization of underwater signals, including recurrent transients under various noise conditions, as well as signal and environmental uncertainties. He was also an early contributor to optimal (likelihood-ratio-based) decision fusion. His recent contributions include the development of physics-based array signal processing algorithms, which incorporate the physics, as well as the uncertainty of ocean acoustic environmental parameters. His current research interests also include the application of signal-detection theory to medical imaging in cancer research in collaboration with the Duke University Medical Center.

Dr. Nolte has served as an associate editor of underwater acoustics for the IEEE TRANSACTIONS ON ACOUSTICS, SPEECH, AND SIGNAL PROCESSING, and has served on its Technical Committee on Underwater Acoustics.

William T. Joines (M'61–SM'94–LSM'97) was born in Granite Falls, NC. He received the B.S.E.E. degree (with high honors) from North Carolina State University, Raleigh, in 1959, and the M.S. and Ph.D. degrees in electrical engineering from Duke University, Durham, NC, in 1961 and 1964, respectively.

From 1959 to 1966, he was a Member of the Technical Staff at Bell Telephone Laboratories, Winston-Salem, NC, where he was engaged in research and development on MW components and systems for military applications. In 1966, he joined the faculty of Duke University, where he is currently a Professor of electrical and computer engineering. His research and teaching interests are in the area of electromagnetic-wave interactions with structures and materials, mainly at MW and optical frequencies. He has authored or co–authored over 100 technical papers on electromagnetic-wave theory and applications and holds seven U.S. patents.

Dr. Joines was the recipient of the Scientific and Technical Achievement Award presented by the Environmental Protection Agency in 1982, 1985, and 1990.